Statistical Analysis of X-ray Speckle at the NSLS

Ophelia K. C. Tsui,[a] S. G. J. Mochrie[a]* and L. E. Berman[b]

[a]*Center for Materials Science and Engineering, Massachusetts Institute of Technology, Cambridge, MA 02139, USA, and* [b]*National Synchrotron Light Source, Brookhaven National Laboratory, Upton, NY 11973, USA. E-mail: simon@lindy.mit.edu*

A statistical analysis of the static speckle produced by illuminating a disordered aerogel sample by a nominally coherent X-ray beam at wiggler beamline X25 at the National Synchrotron Light Source is reported. The results of the analysis show that the coherence delivered to the X25 hutch is within 35% of what is expected. The rate of coherent photons is approximately two times smaller than expected on the basis of the X25 wiggler source brilliance.

Keywords: X-ray speckle; coherent X-rays.

1. Introduction

Insertion-device-based synchrotron X-ray sources present us with the exciting opportunity to carry out X-ray intensity-fluctuation spectroscopy (XIFS) measurements to investigate the dynamics of condensed matter on molecular length scales (Brauer *et al.*, 1995: Dierker, Pindak, Fleming, Robinson & Berman, 1995; Thurn-Albrecht *et al.*, 1996; Mochrie *et al.*, 1997). The success of these experiments, and others requiring coherent X-rays, depends crucially on being able to employ X-ray beams of the highest possible brilliance. In principle, the number of X-ray photons per second in a coherent beam is simply and directly related to the source brilliance. However, in planning XIFS experiments it is imperative to quantify whether the theoretical ideal is achieved at the sample under study. If the brilliance/coherence at the sample under study is less than expected or cannot be fully utilized, steps may then be taken to remedy the situation. We also note that the current interest in 'fourth-generation' synchrotron sources derives in part from novel coherent X-ray experiments, which may become possible with the extreme brilliance of these sources. To make use of a fourth-generation source, the promised coherence must be delivered to the sample under study.

Recently, Abernathy and coworkers (Abernathy *et al.*, 1998) have introduced a method for conveniently quantifying coherence. In brief, a static strongly scattering aerogel sample is illuminated by a coherent X-ray beam, prepared by means of a pinhole, immediately upstream of the sample (Sutton *et al.*, 1991; Cai *et al.*, 1994). The scattered X-rays give rise to the speckle that is characteristic of a disordered medium under partially coherent illumination. The statistical properties of the observed speckle are then analyzed to determine the coherence properties of the illumination. Perfect coherence corresponds to a single mode of the electromagnetic field. It turns out that it is possible to

provide a good description of the experimental statistics of the observed partially coherent X-ray speckle pattern by supposing it to be the intensity sum of several independent 'Gaussian' modes of the electromagnetic field, each of which contributes its own independent perfectly coherent speckle pattern. The number of contributing modes, M, succinctly specifies the coherence of the sample illumination and detection. In this context the variance of the intensity distribution is $\beta = 1/M$, while the often employed second factorial moment is $1 + \beta = 1 + 1/M$. Incoherent illumination corresponds to $M = \infty$, *i.e.* $\beta = 0$. In the context of an XIFS measurement β is the expected zero-time intercept of the normalized baseline-subtracted time autocorrelation function, while the visibility of intensity fluctuations is $\beta^{1/2}$. We will use whichever of β and M seems the most convenient.

In the present paper we follow this procedure to determine the coherence of the beam delivered into the hutch at wiggler beamline X25 at the National Synchrotron Light Source (NSLS). We find that the coherence at X25 is within 35% of the theoretical ideal. However, the rate of coherent photons is about two times smaller than expected. The origin of the discrepancy is uncertain, although beryllium windows are candidates for degrading the source brilliance (Snigirev, Snigireva, Kohn & Kuznetsov, 1996). In addition, there were graphite filters and multilayer monochromator crystals in the beamline. However, the discrepancy here is much smaller than that found in earlier measurements performed at the European Synchrotron Radiation Facility (ESRF) (Abernathy *et al.*, 1998). We do not understand the difference between the NSLS and ESRF results.

The layout of the present paper is as follows. In §2 we describe our experimental methods. In §3 we present the measured aerogel speckle and our analysis of its statistical properties. We draw our conclusions in §4.

2. Experimental details

The layout of beamline X25 pertaining to our experiment is as follows. The source is a 27-pole wiggler, which is 1.6 m long. There is a set of pyrolytic graphite filters, of total thickness 167 µm, 13 m downstream from the source. The first beryllium window, of thickness 254 µm (IF-1 ultra-high purity grade, but unpolished), is 13 m downstream of the graphite filters. X-rays of energy 7 keV within a bandwidth of 1.5% were selected by a vertically diffracting tungsten–boron carbide multilayer pair, located at a distance of 18 m. The multilayers are each known to have a root-mean-square surface roughness of less than 5 Å and a figure error of 2 arcsec or less. The final beryllium window, of thickness 127 µm (IF-1 purity and buff-polished to a root-mean-square surface roughness of 0.4 µm or better on both surfaces), is at a distance of about 26 m. Adjustable slits are located immediately downstream of the second beryllium window, and are set to 4.2 µm in the horizontal and 8.9 µm in the vertical, as determined by measurements of the full width at half maximum (FWHM) of the Fraunhofer diffraction patterns in the horizontal and vertical, respectively (data not shown). Passing through this aperture were $\sim 5 \times 10^7$ nominally coherent photons per second. The aerogel sample, 8 cm downstream of the slits, was the same sample as employed by Abernathy *et al.* (1998) and was kindly supplied by Dr Norbert Mulders of Pennsylvania State University. The sample was contained in an evacuated cell with kapton windows for X-ray access. Between the sample and detector was an evacuated flight path of length 2.3 m, also with kapton windows. The detector, a Princeton Instruments CCD camera employing direct X-ray detection, was located 2.5 m downstream of the sample. The CCD pixel size was 22×22 µm^2. The characteristics of this detector have been analyzed and discussed in detail by Mainville *et al.* (1997).

3. Results

3.1. Aerogel speckle

Fig. 1 shows a rainbow-scale image of the small-angle scattering obtained for a 95%-void aerogel sample. These data are the sum of twenty 100 s exposures, obtained sequentially. The speckle pattern found for each exposure was the same within counting statistics and the time correlation function of the 20 exposures was constant. Therefore, we believe that the incident beam was sufficiently stable during the experiment. The scattering is comprised of a well understood intensity envelope, which is strongly modulated by virtue of the partially coherent illumination. This is speckle. The details of the speckle pattern depend on the exact distribution of material in the aerogel. The axes are labeled by CCD pixel number. The direct beam would occur at pixel (257, −27), in a region of the CCD that is masked by a beam stop to prevent illumination of the CCD by the direct beam. The wavevector range spanned by the illuminated region of the CCD is from −0.0081 to 0.0079 Å^{-1} in the horizontal and from 0.0021 to 0.0173 Å^{-1} in the vertical.

Fig. 2 shows a 64×64 pixels sub-frame centered at a wavevector of 0.006 Å^{-1} in the vertical direction. Inspection of Fig. 2 reveals that the intensity does not fluctuate from pixel to pixel, but rather it varies over a scale of a few pixels. We will quantify this observation below, but we may already be confident that the spatial resolution of the detector does not inadvertently average the intensity fluctuations, *i.e.* the detection preserves the speckle visibility. A striking feature of the speckle is a radial streaking that becomes more
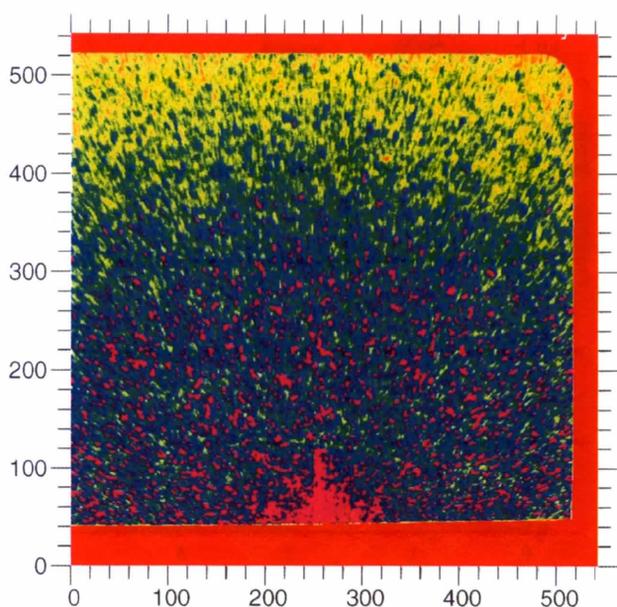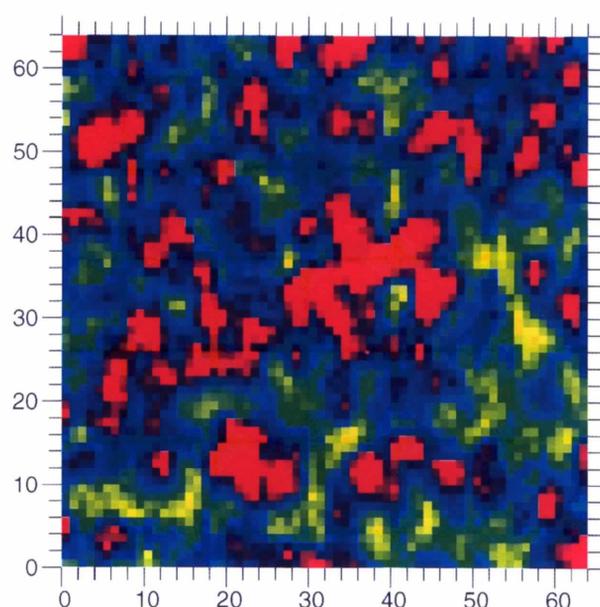

Figure 1
Aerogel speckle pattern.

Figure 2
Detail of the aerogel speckle pattern at 0.006 Å^{-1}.

pronounced at larger scattering wavevectors. This feature is due to the wavelength distribution of the incident beam and will likewise be quantified below. Fig. 3 shows the azimuthally averaged intensity for the speckle shown in Fig. 1. This represents the intensity envelope.

3.2. Probability density of the speckle intensity

The most characteristic feature of speckle is the large point-to-point intensity variation, as evidenced in Fig. 1. Figs. 4(a) and 4(b) show the probability density of the speckle intensity determined from sub-frames of 64×64 pixels $(0.002 \times 0.002 \text{ Å}^{-2})$ centered at wavevectors of 0.006 and 0.016 Å^{-1}, respectively, obtained by histogramming the observed intensities and normalizing by the respective mean intensities of the different regions. The insets show the intensity distributions on a logarithmic scale. As might be anticipated, there is a wide distribution of intensity, far wider than would be expected for counting statistics. Over the range of wavevectors included in each sub-frame, the intensity of the scattering envelope is approximately constant for wavevectors less that 0.01 Å^{-1}. Above 0.01 Å^{-1} the intensity changes with Q by a noticeable amount. However, within the wavevector range of each sub-frame the variation is no more than about 12% from its mean. We found that for a sub-frame taken about Q = 0.016 Å^{-1}, where it is most susceptible to this error, the result is essentially unchanged by first normalizing the region by the intensity envelope. Therefore, we conclude that throughout the wavevector range we have studied the intensity envelope makes no contribution to the width of the intensity distribution.

The speckle produced by a coherent (single-mode) source is expected to display an exponential intensity distribution, i.e. $p_1(I) = (1/\bar{I})\exp(-I/\bar{I})$ (Goodman, 1975), as a result of a Gaussian distribution of the electromagnetic field strength
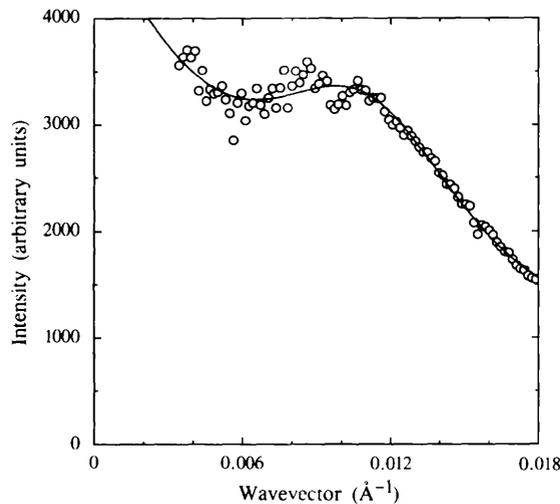
about zero: because the field strength of the scattered wave at a point in space consists of contributions from each of the many electrons in the sample, the central limit theorem of statistics implies a Gaussian distribution of field strength. Evidently, the experimental distributions in Fig. 4 do not conform to this form. However, let us suppose that the observed partially coherent speckle may be considered to be the intensity sum of M independent coherent speckle patterns, each with the same field strength, i.e. M modes of the electromagnetic field contribute to the observed intensity. It can be easily derived that the probability density of the intensity in this case is given by (Goodman, 1975)

$$p_M(I) = \int \delta\left(I - \sum_{j=1}^{j=M} I_j\right) \prod_{j=1}^{j=M} p_1(I_j) \, dI_j$$

$$= M^M (I/\bar{I})^{M-1} \exp(-MI/\bar{I})/[\Gamma(M)\bar{I}]. \quad (1)$$

The distribution of intensity described by (1) has mean $\bar{I}$ and standard deviation $\sigma_I = \bar{I}/M^{1/2}$. This latter result implies that the speckle visibility is $1/M^{1/2} = \beta^{1/2}$ for an intensity distribution described by (1).

Equation (1) is formally sensible for non-integer values of M. The solid lines in Fig. 4 show the best fit of (1) with variable M to the experimental data. The values of M (β) so-obtained are ~ 6 (~ 0.17) and ~ 11 (~ 0.08) for 0.006 and 0.016 Å^{-1}, respectively. Inspection of Fig. 4 reveals that the model peaks at an intensity that is slightly higher than the peak of the actual distribution. Overall, however, the model form provides a good description of the experimental distributions. Fig. 5 shows the best-fit values of M plotted
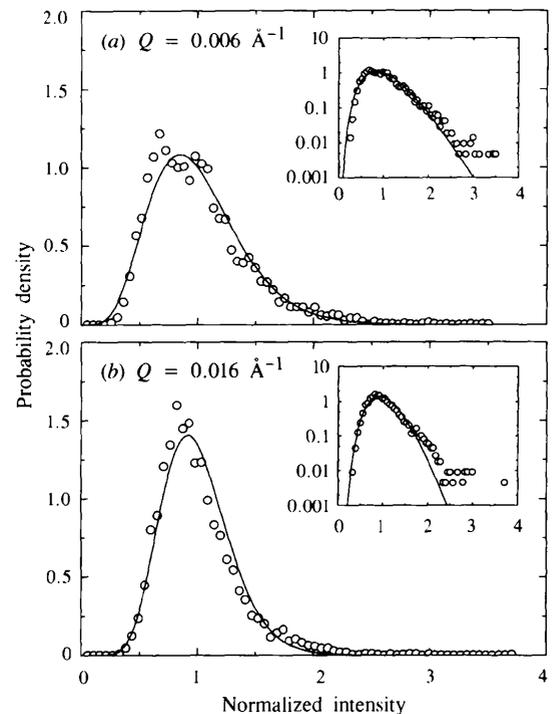
Figure 3
Aerogel scattering intensity *versus* wavevector obtained by azimuthally averaging the CCD image of Fig. 1 (open circles). The line is a guide to the eyes.

Figure 4
Probability density of the speckle intensity: (a) 0.006 and (b) 0.014 Å^{-1}.

versus wavevector for the distributions of Fig. 4 and for analogous distributions obtained at intermediate wavevectors.

3.3. *Speckle-intensity autocorrelation*

To quantify the speckle visibility independently of a model, to quantify the speckle size and to demonstrate that Poisson counting statistics do not play a role in the observed intensity distributions, we may calculate the autocorrelation of the speckle between different pixels. Figs. 6(a) and 6(b) show the normalized autocorrelation *versus* pixel separation in the radial and tangential directions for the sub-frames centered at 0.006 and 0.014 Å^{-1}, respectively. It is worth noting that the autocorrelation in the limit of zero pixel separation is $1 + \sigma_I^2/\bar{I}^2 = 1 + \beta$. We believe that the deviation of the autocorrelation from unity far from zero reflects incomplete averaging as a result of the limited size of the sub-frame considered (64 × 64 pixels).

The normalized autocorrelation was calculated in two ways. First, the 20 exposures were summed together and the normalized autocorrelation of the summed image was calculated. The results for the radial and tangential correlations are shown as open circles and open triangles, respectively. Second, the normalized autocorrelation of each exposure was calculated. The results of averaging the 20 individual normalized autocorrelations in the radial direction are shown as solid circles. Evidently, the autocorrelations in the radial direction obtained in these different ways overlap, except near zero. The same is true for the tangential direction (data not shown for the second method).

The difference between the autocorrelations obtained by the two methods originates in the 20-times-larger contribution of Poisson counting statistics to the intensity fluctuations for the second method. Specifically, since the Poisson
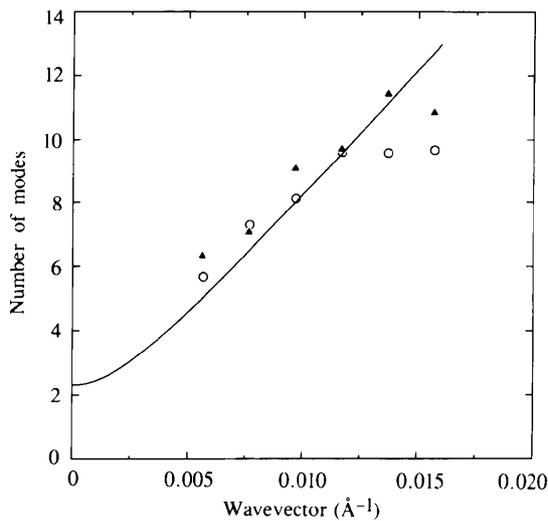
contribution to the variance is given by the number of photons counted (Mainville *et al.*, 1997), the difference between the two autocorrelations divided by the autocorrelation at large displacements has an (integrated) amplitude equal to 19/20 times the inverse of the average number of photons per pixel per 100 s counting time (Dufresne, Brüning, Sutton, Rodricks & Stephenson, 1995). Thus, for example, near 0.006 Å^{-1} there were approximately six X-ray photons per pixel per 100 s. By examining the unnormalized autocorrelation we may deduce that there are approximately 630 detector units per 7 keV X-ray photon. This result, *i.e.* 90 detector units per keV, agrees well with the earlier more detailed analysis of Mainville *et al.* (1997), which deduced 94 detector units per keV from measurements using 8.3 keV X-ray photons.

It is clear from Fig. 6 that Poisson counting statistics do not contribute significantly to the autocorrelation of the summed image. Therefore, the autocorrelation of the summed image reflects accurately the speckle size and the speckle visibility. On this basis we may infer that counting statistics do not contribute significantly to the intensity distributions of Fig. 4. The open circles in Fig. 5 correspond to the values of M determined from $1/M = \sigma_I^2/\bar{I}^2$ for the summed image autocorrelation at zero pixel separation. They agree well with the values deduced from the fits to the model intensity distributions (see Fig. 5).

It is important to note that the Poisson contribution to the autocorrelation directly determines the detector resolution, *i.e.* the amount of 'cross-talk' between neighboring pixels. For the autocorrelations near 0.006 Å^{-1} the Poisson

Figure 5
Number (M) of modes contributing to the observed partially coherent speckle pattern *versus* wavevector. Data were determined from fits to the intensity distribution with variable M (solid triangles), and from the speckle autocorrelation (open circles).
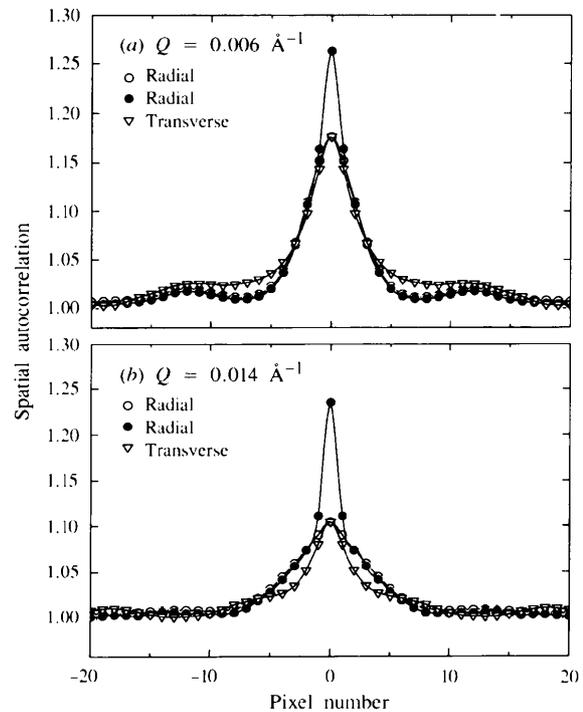
Figure 6
Normalized autocorrelation *versus* pixel separation in the radial (open and solid circles) and tangential (open triangles) directions near (a) 0.006 and (b) 0.014 Å^{-1}.

contribution to the autocorrelation displays an FWHM of one pixel, and the speckle contribution to the autocorrelation displays an FWHM of four pixels. It follows that the effective detector resolution is indeed much smaller than the speckle size, and does not significantly diminish the observed intensity fluctuations. Since the speckle autocorrelation widths increase with wavevector, this will also be true at larger wavevectors than 0.006 Å^{-1}.

In Fig. 6 it may be seen that the tangential width is approximately the same at the two wavevectors shown, but that the radial width is considerably larger at the larger wavevector, reflecting the observed radial streaking of the speckle, seen in Fig. 1. This observation is quantified in Fig. 7, which shows the FWHM of the background-subtracted normalized autocorrelation in the radial and tangential directions.

4. Discussion and conclusions

We now discuss what may be expected for the FWHM of the background-subtracted autocorrelation for our experimental configuration. In our case the tangential direction is horizontal and the radial direction is vertical. Therefore, the FWHM of the background-subtracted autocorrelation (in wavevector) in the tangential direction is expected to be (Goodman, 1975)

$$\delta Q_\theta \simeq 5.57/d_h, \tag{2}$$

where $d_h = 4.2$ μm is the horizontal slit size. Because the effective vertical size of the scattering volume increases with increasing scattering angle, the speckle width in the vertical (radial) direction tends to decrease with increasing wavevector (Chu, 1974). However, in the case where the bandwidth is non-zero, the intensity in a given speckle, which is actually at a fixed wavevector, becomes distributed
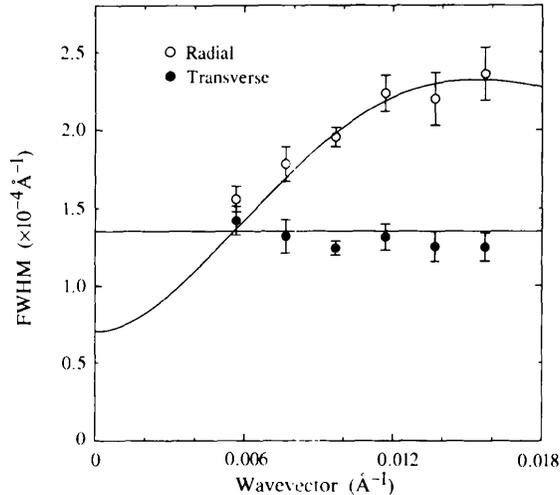

Figure 7
FWHM of the background-subtracted autocorrelation in the radial (open circles) and tangential (solid circles) directions *versus* wavevector.

over a range of scattering angles corresponding to the wavelength distribution. This tends to increase the speckle width in the radial (vertical) direction. On the basis of a Gaussian approximation for the scattering volume and spectral distribution, Abernathy *et al.* (1998) have derived that the variation of the speckle radial width with wavevector is given by

$$\delta Q_r \simeq 5.57 \left[\frac{1 + (0.064 d_v^2 Q^2 + 0.016 W^2 Q^4/k^2)(\delta\lambda/\lambda)^2}{d_v^2 + W^2 Q^2/k^2 + 0.016 d_v^2 W^2 Q^4 (\delta\lambda/\lambda)^2/k^2} \right]^{1/2}, \tag{3}$$

where d_v is the vertical slit size and W is the sample thickness (nominally 0.6 mm). The FWHMs predicted on the basis of (2) and (3) are shown in Fig. 7 as solid lines. The model provides a good description of the experimental results.

Abernathy *et al.* (1998) have also derived that the number of modes increases with wavevector according to

$$M = M_0[1 + (0.064 d_v^2 Q^2 + 0.016 W^2 Q^4/k^2)(\Delta\lambda/\lambda)^2]^{1/2}. \tag{4}$$

This form, with $M_0 = 2.3$, is shown as the solid line in Fig. 5. Evidently, (4) provides a fair description of the wavevector dependence of the experimental data. It is worthwhile to compare the current result with earlier discussions (Dierker *et al.*, 1995; Thurn-Albrecht *et al.*, 1996; Mochrie *et al.*, 1997; Abernathy *et al.*, 1998; Mainville *et al.*, 1997), which suggests that the maximum optical path-length difference should be less than the longitudinal coherence length. This notion, in turn, leads to the conditions $\lambda^2/\Delta\lambda \geq d_v Q/k$ and $\lambda^2/\Delta\lambda \geq W Q^2/k^2$. Formulated in the context of (4), these conditions result in the criterion $M \leq 2M_0$ under our experimental configuration, so that $\lambda^2/\Delta\lambda \geq (2.52 d_v^2 Q^2/k^2 + 0.63 W^2 Q^4/k^4)^{1/2}$. As Fig. 5 shows, this criterion is not satisfied in the range of Q that we have studied, although the speckles are visible. As for dynamical measurements, we were able to undertake XIFS studies of colloidal suspensions for values of M up to 11 using the current setup (Tsui & Mochrie, 1997). It follows that the conditions set based on considerations of optical path differences are too stringent in accessing the feasibility of an XIFS experiment.

It remains to discuss what may be expected for M_0. In consideration of the optical speckle produced by perfectly coherent laser illumination, one is generally interested in the coherence area of the illuminated sample volume at the detector, relative to the detector area. Under these circumstances the number of modes which contribute to the observed speckle statistics is given by the ratio of the detector area to the coherence area of the illuminated sample volume at the detector. In our case the illuminated sample volume is determined by the slits immediately upstream of the sample, and, as shown above, the detector resolution is smaller than the coherence area in question, so that the detection scheme is essentially coherent.

However, our source is not perfectly coherent, and to determine how many modes may be expected to contribute to the observed intensity distribution, as a result of finite source size, we may compare the coherence area of the source at the slit location with the actual slit area. Under these circumstances the number of modes contributing to the observed speckle statistics is given by the ratio of the slit area to the source coherence area at the slit location (Pusey, 1977). More precisely, we should compare the source horizontal and vertical coherence lengths, respectively, with the horizontal and vertical sizes, respectively, of the slits.

To develop the appropriate quantitative comparison we employ several results given by Goodman (1975). We will initially consider a one-dimensional source with a Gaussian intensity distribution given by

$$I(s) = I(0) \exp(-\pi s^2 / l^2), \tag{5}$$

where s is a coordinate in the plane of the source and l specifies the source size. Then, the number of modes transmitted through a slit of width d at distance R for X-rays of wavelength λ is

$$M_0 = \{(\xi/d)\, \mathrm{erf}(\pi^{1/2}d/\xi)$$
$$- (\xi^2/\pi d^2)[1 - \exp(-\pi d^2/\xi^2)]\}^{-1}, \tag{6}$$

where $\xi = \lambda R/l$ is the coherence length (Goodman, 1975). Fig. 8 shows the number of modes according to (6) plotted *versus* d/ξ. For $d/\xi \geq 2$ the number of modes is well approximated by $M_0 \simeq d/\xi + 0.37$.

In the case of the actual two-dimensional source the number of contributing modes is the product of two such terms, one for the horizontal direction (M_h) and one for the vertical direction (M_v), *i.e.* $M_0 = M_v M_h$. The nominal 2σ vertical and horizontal source sizes at the NSLS are 17 and 820 µm, respectively, at the center of the wiggler. However, because of the non-zero divergence of the electron beam

along the length of the wiggler, the effective 2σ vertical and horizontal source widths are estimated to be 36 and 1057 µm, respectively. Assuming a Gaussian intensity distribution across the source, it follows that the vertical and horizontal source sizes are $l_v = 45$ µm and $l_h = 1325$ µm, respectively, so that the vertical and horizontal coherence lengths are $\xi_v = \lambda R/l_v = 99$ µm and $\xi_h = \lambda R/l_h = 3.3$ µm, respectively. For the vertical direction, $d_v/\xi_v \simeq 0.09$, and we expect $M_v \simeq 1$; for the horizontal direction, $d_h/\xi_h \simeq 1.3$, and we expect $M_h \simeq 1.7$. Thus, we expect $M_0 \simeq 1.7$. In fact, our data extrapolate to $M_0 \simeq 2.3$, which is only 35% larger than expected.

Finally, it is important to compare the observed rate of coherent X-ray photons with the value expected on the basis of the expected brilliance of the X25 wiggler source, which is 2×10^{16} X-rays (0.1% bandwidth)$^{-1}$ s^{-1} mm^{-2} mrad^{-2} at a ring current of 200 mA, *i.e.* 3×10^9 X-rays (1.5% bandwidth)$^{-1}$ s^{-1} Å^{-2} rad^{-2}. The rate of coherent X-ray photons, R_{coh}, is the fraction of the total rate, R_{tot}, that is emitted into the coherence area of the source, *i.e.* $R_{coh} = R_{tot} (\lambda/l_v\theta_v)(\lambda/l_h\theta_h) = \lambda^2 B = 8 \times 10^9$ coherent X-ray photons s^{-1}, where θ_v and θ_h are the opening angles of the wiggler in the vertical and horizontal directions, respectively, and B is the brilliance. We should not expect to realize this rate in the present experiment, in part, because the vertical coherence length (99 µm) is larger by a factor of 11 than the vertical slit size (8.9 µm). In addition, because of filters, beryllium windows and air in the X-ray path, there may be a factor of 3 (at most) attenuation along the beamline, and the reflectivity of the multilayer pair is 50%. Thus, we should ideally expect 1×10^8 coherent photons s^{-1}. This may be compared with 4 $\times 10^7$ photons passing our slits.

In conclusion, we have performed a statistical analysis of speckle from an aerogel sample produced at beamline X25 at the NSLS. The experimental scheme described here provides a convenient means to monitor the coherence of an X-ray beam. The results indicate that the coherence is within 35% of what is expected, and that the number of coherent photons is a factor of about two smaller than expected on the basis of the expected brilliance. Finally, a number of formulae have been collected that may be helpful in considerations of the feasibility and optimization of XIFS studies using large-bandwidth radiation.

Figure 8
Number of speckle patterns (number of modes) *versus* d/ξ, according to equation (6).

References

Abernathy, D. L., Grübel, G., Brauer, S., McNulty, I., Stephenson, G. B., Mochrie, S. G. J., Sandy, A. R., Mulders, N. & Sutton, M. (1998). *J. Synchrotron Rad.* **5**, 37–47.
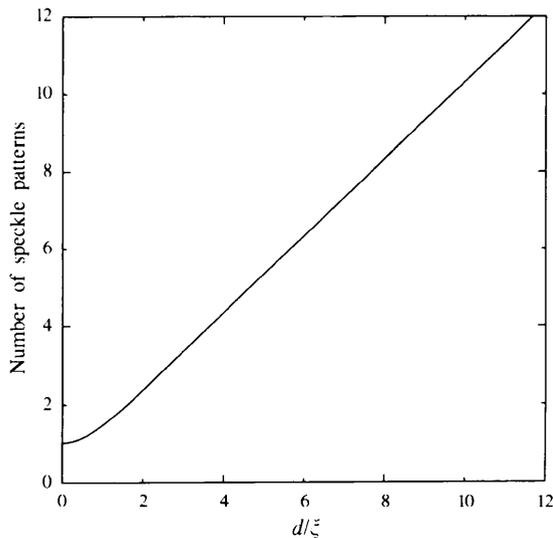
Brauer, S., Stephenson, G. B., Sutton, M., Brüning, R., Dufresne, E., Mochrie, S. G. J., Grübel, G., Als-Nielsen, J. & Abernathy, D. L. (1995). *Phys. Rev. Lett.* **74**, 2010–2013.

Cai, Z. H., Lai, B., Yun, W. B., McNulty, I., Huang, K. G. & Russell, T. P. (1994). *Phys. Rev. Lett.* **73**, 82–85.

Chu, B. (1974). *Laser Light Scattering.* Orlando: Academic Press.

Dierker, S., Pindak, R., Fleming, R. M., Robinson, I. K. & Berman, L. E. (1995). *Phys. Rev. Lett.* **75**, 449–452.

Dufresne, E., Brüning, R., Sutton, M., Rodricks, B. & Stephenson, G. B. (1995). *Nucl. Instrum. Methods,* **A364**, 380–393.

Goodman, J. W. (1975). In *Laser Speckle and Related Phenomena,* edited by J. C. Dainty. Heidelberg: Springer-Verlag.

Mainville, J., Bley, F., Livet, F., Geissler, E., Legrand, J. F., Abernathy, D., Grübel, G., Mochrie, S. G. J. & Sutton, M. (1997). *J. Appl. Cryst.* **30**, 828–832.

Mochrie, S. G. J., Mayes, A. M., Sandy, A. R., Sutton, M., Brauer, S., Stephenson, G. B., Abernathy, D. L. & Grübel, G. (1997). *Phys. Rev. Lett.* **78**, 1275–1278.

Pusey, P. N. (1977). In *Photon Correlation Spectroscopy and Velocimetry,* edited by H. Z. Cummins & E. R. Pike. New York: Plenum.

Snigirev, A., Snigireva, I., Kohn, V. G. & Kuznetsov, S. M. (1996). *Nucl. Instrum Methods,* **A370**, 634–640.

Sutton, M., Mochrie, S. G. J., Greytak, T., Nagler, S. E., Berman, L. E., Held, G. A. & Stephenson, G. B. (1991). *Nature (London),* **352**, 608–610.

Thurn-Albrecht, T., Steffen, W., Patkowski, A., Meier, G., Fisher, E. W., Grübel, G. & Abernathy, D. L. (1996). *Phys. Rev. Lett.* **77**, 5437–5440.

Tsui, O. K. C. & Mochrie, S. G. J. (1997). Unpublished.